Extracting Angular Correlations from the Rare Decay $\overline{B}_d \to \overline{K}^{*0}\mu^+\mu^-$ at LHC*b*

William Reece[1,*]

(on behalf of the LHC*b* collaboration)

[1] *Imperial College London*

$\overline{B}_d \to \overline{K}^{*0}\mu^+\mu^-$ is a rare flavour changing neutral current decay. It proceeds via a $b \to s$ quark transition and is sensitive to many classes of new physics model. In this article the theoretical framework relevant to making a measurement at LHC*b*, the precision flavour experiment at the Large Hadron Collider, will be introduced. Progress made towards using a full angular analysis to extract $A_{\rm FB}$, the forward–backwards asymmetry of the μ pair, will be covered and its implications for the $A_{\rm FB}$ zero–crossing point discussed.

PACS numbers: 13.20.He.

1. INTRODUCTION

Since its inception, the Standard Model (SM) of electroweak and strong interactions has been able to describe the available physics data with impressive accuracy. When the Large Hadron Collider (LHC) starts later this year at CERN, we will be able to test SM predictions at a new energy scale far above m_W, the mass of the W gauge boson. There are well known reasons, such as the hierarchy problem and the existence of dark matter, to think that the SM will break down at these new scales, perhaps revealing new information about the interactions of particles beyond the electroweak scale.

A major aim of the LHC is to discover these new physical interactions and to probe their nature. There are two main approaches to these new physics (NP) searches; direct or indirect. In this article we will discuss preparations for an indirect NP search with the LHC*b* detector in the rare decay $\overline{B}_d \to \overline{K}^{*0}\mu^+\mu^-$.

* w.reece06@imperial.ac.uk

The rest of this article is laid out as follows. In the next section we start by introducing the decay. In Sec. 3 we briefly review the operator product expansion (OPE) then discuss angular observables. In Sec. 4 we discuss the sensitivity to one of these observables at LHCb, using a full angular analysis. Finally in Sec. 5 we summarise our findings and present an outlook for the future.

2. $\overline{B}_d \to \overline{K}^{*0}\mu^+\mu^-$

$\overline{B}_d \to \overline{K}^{*0}\mu^+\mu^-$ is a flavour changing neutral current (FCNC) $b \to s$ quark transition decay that proceeds at the one–loop level via penguin and box diagrams such as the SM diagrams shown in Fig. 1. It was first observed at BELLE [1] and has a branching ratio of $(1.22^{+\ 0.38}_{-\ 0.32}) \times 10^{-6}$ [2]. The decay is sensitive to NP contributions through new diagrams where charged or neutral NP particles run in the loop [3–6]. Studies show [7] that the decay can be selected at LHCb giving approximately 4032 signal and 1168 background events per $2\,\text{fb}^{-1}$ in the range $4m_\mu^2 \leq q^2 \leq 9\,\text{GeV}^2/c^4$, where q^2 is the invariant mass of the muon pair. These yield estimates correspond to $1 \times 10^7\,\text{s}$ of stable LHC running[1].

In this article we will deal explicitly with only the decay of the $\overline{B}_d$. Assuming a SM–like scenario where CP violation can be neglected we can consider the B_d and $\overline{B}_d$ simultaneously once appropriate redefinitions have been made. Following Ref. [9], we treat the $\overline{K}^{*0}$ as delta–function so that it always decays on its mass shell to a K^- and a π^+. In this approximation the decay can be kinematically constrained by q^2 and three angles, θ_l, θ_K, and ϕ. The angles are defined in the intervals

$$0 \leqslant \theta_l \leqslant \pi\,, \quad 0 \leqslant \theta_K \leqslant \pi\,, \quad -\pi \leqslant \phi < \pi\,, \tag{1}$$

where in particular it should be noted that the ϕ angle is signed. The decay kinematics are shown in Fig. 2 and the definitions of the angles are given in the caption. We work in the massless leptons approximation for which we can derive a simplified differential decay width for the $\overline{B}_d$,

$$\frac{d^4\Gamma_{\overline{B}_d}}{dq^2\,d\theta_l\,d\theta_K\,d\phi} = \frac{9}{32\pi} I(q^2, \theta_l, \theta_K, \phi) \sin\theta_l \sin\theta_K\,, \tag{2}$$

[1] Theoretical considerations limit us to the range $1 \leq q^2 \leq 6\,\text{GeV}^2/c^4$ and so these estimates must be scaled appropriately into this range as in Ref. [8].

where a sum over final state particle spins has been included, the physical region of phase space is $4m_\mu^2 \leqslant q^2 \leqslant (m_B - m_{\overline{K}^{*0}})^2$ and

$$\begin{aligned} I &= I_1 + I_2\cos 2\theta_l + I_3 \sin^2\theta_l \cos 2\phi + I_4 \sin 2\theta_l \cos\phi + I_5 \sin\theta_l \cos\phi + I_6 \cos\theta_l \\ &+ I_7 \sin\theta_l \sin\phi + I_8 \sin 2\theta_l \sin\phi + I_9 \sin^2\theta_l \sin 2\phi. \end{aligned} \tag{3}$$

For the B_d we use $\bar{I}(q^2, \theta_l, \theta_K, \phi)$ where $I_{1,2,3,4,6,7} = \bar{I}_{1,2,3,4,6,7}$ and $I_{5,8,9} = -\bar{I}_{5,8,9}$. The functions I_{1-9} in Eq. (3) can be written in terms of the transversity amplitudes A_0, $A_\parallel$, $A_\perp$, A_t which all have both left and right handed components and are functions of q^2. A_t corresponds to the scalar component of the virtual $\overline{K}^{*0}$, which is negligible if the μ mass is small in comparison to the invariant mass of the μ pair. Neglecting A_t and setting $m_\mu = 0$ we find from [9]

$$I_1 = \frac{3}{4}\left(|A_{\perp L}|^2 + |A_{\parallel L}|^2 + (L \to R)\right)\sin^2\theta_K + \left(|A_{0L}|^2 + |A_{0R}|^2\right)\cos^2\theta_K, \tag{4a}$$

$$I_2 = \frac{1}{4}(|A_{\perp L}|^2 + |A_{\parallel L}|^2)\sin^2\theta_K - |A_{0L}|^2\cos^2\theta_K + (L \to R), \tag{4b}$$

$$I_3 = \frac{1}{2}\Big[(|A_{\perp L}|^2 - |A_{\parallel L}|^2)\sin^2\theta_K + (L \to R)\Big], \tag{4c}$$

$$I_4 = \frac{1}{\sqrt{2}}\Big[\Re(A_{0L}A_{\parallel L}^*)\sin 2\theta_K + (L \to R)\Big], \tag{4d}$$

$$I_5 = \sqrt{2}\Big[\Re(A_{0L}A_{\perp L}^*)\sin 2\theta_K - (L \to R)\Big], \tag{4e}$$

$$I_6 = 2\Big[\Re(A_{\parallel L}A_{\perp L}^*)\sin^2\theta_K - (L \to R)\Big], \tag{4f}$$

$$I_7 = \sqrt{2}\Big[\Im(A_{0L}A_{\parallel L}^*)\sin 2\theta_K - (L \to R)\Big], \tag{4g}$$

$$I_8 = \frac{1}{\sqrt{2}}\Big[\Im(A_{0L}A_{\perp L}^*)\sin 2\theta_K + (L \to R)\Big], \tag{4h}$$

$$I_9 = \Big[\Im(A_{\parallel L}^*A_{\perp L})\sin^2\theta_K + (L \to R)\Big], \tag{4i}$$

where the $(L \to R)$ terms represent a repeat of the previous terms with the left handed amplitudes exchanged for right handed. It is by extracting the values of these amplitudes that we can try to detect the effects of physics beyond the SM. This is investigated further in the next section.

3. ANGULAR OBSERVABLES

A major advantage of the indirect approach to NP searches is that it allows the use of model independent techniques such as the operator product expansion (OPE). OPE allows the SM to be parameterised into an effective theory made up of effective vertices and their coupling constants, known as the Wilson coefficients. For $b \to s\ell^+\ell^-$ quark transitions the decay amplitude can be written in terms of an effective Hamiltonian

$$\mathcal{H}_{\rm eff} = -\frac{4G_{\rm F}}{\sqrt{2}} V_{\rm tb} V_{\rm ts}^* \sum_{i=1}^{10} \left[C_i(\mu)\mathcal{O}_i(\mu) + C_i'(\mu)\mathcal{O}_i'(\mu) \right] \tag{5}$$

where $V_{\rm tb}$ and $V_{\rm ts}$ are the numerically dominant CKM [10] factors and, following the conventions of Ref. [9], primes (no primes) denote right–handed (left–handed) contributions. The local operators $\mathcal{O}_i(\mu)$ describe the long range contributions to the decay while the short range contributions, coming from integrated out heavy degrees of freedom, are parameterised by the Wilson coefficients $C_i(\mu)$. μ is the renormalisation scale at which the decay is treated; typically this is $\mathcal{O}(m_b)$.

$\overline{B}_d \to \overline{K}^{*0}\mu^+\mu^-$ is dominated by the Wilson coefficients C_7, C_9 and C_{10}, the right–handed versions of which are heavily suppressed in the SM. The presence of new and unaccounted for heavy degrees of freedom will shift their values away from SM predictions. Additional NP effects can be included in a model independent way by the consideration of non–SM operators, for example parameterising possible scalar contributions. By measuring the values of the Wilson coefficients we can make a model independent test of the SM, and also powerfully exclude general classes of NP. Both *BABAR* and Belle have published measurements [11, 12] but the current experimental constraints on NP are still modest [13, 14]. The large increase in statistics [7] at LHCb for $\overline{B}_d \to \overline{K}^{*0}\mu^+\mu^-$ will make much higher precision measurements possible for the first time, but careful choices of observables need to be made to take full advantage of this.

3.1. Observables

The Wilson coefficients cannot be measured directly, but we can gain sensitivity to them by looking at carefully constructed combinations of the transversity amplitudes, which are themselves functions of the Wilson coefficients. We need to find observables with sensitivity

to NP operators, small theoretical uncertainties and good experimental resolutions. The main source of theoretical uncertainty comes from the soft form factors that parameterise the $\overline{B}_d \to \overline{K}^{*0}$ transition and also enter into the transversity amplitude expressions. At leading order (LO), relationships between the relevant form factor components can be used to form variables where the form factors cancel out, much reducing the overall theoretical uncertainty [3].

In this article we focus our attention on $A_{\rm FB}$, the asymmetry in the number of muons going in the forward and backwards directions, which can be expressed in terms of the transversity amplitudes as

$$A_{\rm FB} = \frac{3}{2}\frac{\Re(A_{\parallel L}A^*_{\perp L}) - \Re(A_{\parallel R}A^*_{\perp R})}{|A_0|^2 + |A_\parallel|^2 + |A_\perp|^2}. \tag{6}$$

The $A_{\rm FB}$ SM distribution, generated with an updated next–to–leading order (NLO) SM calculation based on Ref. [15] (See Acknowledgments), is shown in Fig. 3(a). The point in this distribution where $A_{\rm FB} = 0$ is known as the zero–crossing point and has no form factor uncertainty at LO, due to the cancellations described above. This has been studied in various NP models, and has been found to undergo changes in the presence of NP [3, 16]. The zero–crossing point can be measured at LHCb with low statistics and will be one of the first physics measurements to be made of the $\overline{B}_d \to \overline{K}^{*0}\mu^+\mu^-$ decay [17].

4. SENSITIVITY AT LHCb

To estimate the sensitivity to angular observables such as $A_{\rm FB}$, a toy Monte–Carlo model of the decay was created using Eq. (2) as a probability density function (PDF), normalised with the total width, $\frac{d\Gamma}{dq^2}$. We assume that any non–resonant contributions to $\overline{B}_d \to K^-\pi^+\mu^+\mu^-$ and all detector effects can be neglected. In addition a simplified background model which is flat in all angles is included. This allows different fitting techniques to be evaluated in a simplified but still somewhat realistic environment, although we know from Ref. [17] that these effects will have to be considered more carefully in a final LHCb analysis. The model can be used to generate toy experimental data, an example of which is shown in Fig. 4 for $2\,{\rm fb}^{-1}$ of integrated luminosity, which can then be fit in order to extract the original inputs and then angular observables of interest. If this process is repeated many times, the experimental resolutions on each of the observables can be found, and any biases introduced can be identified. Input values of the transversity amplitudes were taken from

the NLO SM calculation discussed above.

Results from this full angular model were compared with a projection model [8], in which Eq. (2) is integrated with respect to two of the three angles, giving expressions for $\frac{d^2\Gamma}{dq^2 d\theta_L}$, $\frac{d^2\Gamma}{dq^2 d\theta_K}$ and $\frac{d^2\Gamma}{dq^2 d\phi}$, which are then used as PDFs. The treatment of background and detector effects is the same as in the full angular model. These projection fits are one standard way of extracting $A_{\rm FB}$, and so provide a good benchmark when evaluating the full angular technique.

The $A_{\rm FB}$ zero–crossing point can be extracted by finding the value of $A_{\rm FB}$ in several q^2 bins across the momentum spectrum and then fitting a straight line to the bins either side of the crossing point [17]. Fig. 3(a) shows a comparison between the full angular and projection approaches for 1000 toy fits, each to $10\,{\rm fb}^{-1}$ of SM toy data, where the SM input distribution is also shown. The agreement between the input distribution and the output data points for both approaches is excellent. As can be seen by comparing the projected experimental resolutions shown in Fig. 3(b), the resolutions produced by the full angular approach are 30–50% smaller than for the projection approach in the same q^2 bin. If a straight line fit is made to these points to extract the zero–crossing point then the improved resolutions on each point for the full angular approach lead to a similar improvement on the zero–crossing point uncertainty. This simple analysis is too naïve to draw firm quantitative conclusions, however it seems that the full angular approach is worth further consideration for a $A_{\rm FB}$ zero–crossing point measurement at LHCb. It is clear however that the full angular fit can not be used for very small data sets; those with less than $\mathcal{O}(100)$ signal events in each q^2 bin. It seems likely that a first measurement at LHCb will be made using an alternative method, with the full angular approach being used in a later second measurement with a larger data set.

5. CONCLUSIONS

With the impending start of the LHC and the impressive legacy of the B–factories now is an exciting time for B–physics. If there is NP to be discovered at the LHC, $b \to s$ quark transitions will provide an excellent hunting ground, allowing searches to be done in a model independent way. The angular distribution of $\overline{B}_d \to \overline{K}^{*0}\mu^+\mu^-$ provides many opportunities in this area with a set of observables, including the $A_{\rm FB}$ zero–crossing point,

which have good sensitivity to NP, small theoretical uncertainties and excellent experimental prospects at LHCb. Two different means of extracting $A_{\rm FB}$ from the angular distribution of $\overline{B}_d \to \overline{K}^{*0}\mu^+\mu^-$ have been discussed and it was found that the full angular technique can produce significantly smaller experimental resolutions for the same toy data set sizes. This has as yet unquantified implications for the $A_{\rm FB}$ zero–crossing point but it is expected that significant improvements on the zero–crossing point resolution can be made over the standard projection approach once LHCb data sets have grown large enough to perform the fit robustly.

ACKNOWLEDGMENTS

The work presented in this article was done in collaboration with U. Egede, T. Hurth, J. Matias and M. Ramon. The author would like to thanks the organisers of the 36^{th} ITEP winter school for an excellent experience in Moscow and for the convivial atmosphere they strived to create.

---

1. A. Ishikawa et al. (Belle), Phys. Rev. Lett. **91**, 261601 (2003), arXiv:hep-ex/0308044.
2. W. M. Yao et al. (Particle Data Group), J. Phys. **G33**, 1 (2006).
3. A. Ali, P. Ball, L. T. Handoko, and G. Hiller, Phys. Rev. **D61**, 074024 (2000), arXiv:hep-ph/9910221.
4. C. Bobeth, T. Ewerth, F. Kruger, and J. Urban, Phys. Rev. **D64**, 074014 (2001), arXiv:hep-ph/0104284.
5. P. Colangelo, F. De Fazio, R. Ferrandes, and T. N. Pham, Phys. Rev. **D73**, 115006 (2006), arXiv:hep-ph/0604029.
6. E. Lunghi and J. Matias, JHEP **04**, 058 (2007), arXiv:hep-ph/0612166.
7. J. Dickens, V. Gibson, C. Lazzeroni, and M. Patel (2007), CERN-LHCb-2007-038.
8. U. Egede (2007), CERN-LHCb-2007-057.
9. F. Kruger and J. Matias, Phys. Rev. **D71**, 094009 (2005), arXiv:hep-ph/0502060.
10. M. Kobayashi and T. Maskawa, Prog. Theor. Phys. **49**, 652 (1973).
11. B. Aubert et al. (*BABAR*), Phys. Rev. **D73**, 092001 (2006), arXiv:hep-ex/0604007.
12. A. Ishikawa et al. (Belle), Phys. Rev. Lett. **96**, 251801 (2006), arXiv:hep-ex/0603018.

13. P. Gambino, U. Haisch, and M. Misiak, Phys. Rev. Lett. **94**, 061803 (2005), arXiv:hep-ph/0410155.
14. G. Hiller and F. Kruger, Phys. Rev. **D69**, 074020 (2004), arXiv:hep-ph/0310219.
15. M. Beneke, T. Feldmann, and D. Seidel, Nucl. Phys. **B612**, 25 (2001), arXiv:hep-ph/0106067.
16. T. Feldmann and J. Matias, JHEP **01**, 074 (2003), arXiv:hep-ph/0212158.
17. J. Dickens, V. Gibson, C. Lazzeroni, and M. Patel (2007), CERN-LHCb-2007-039.

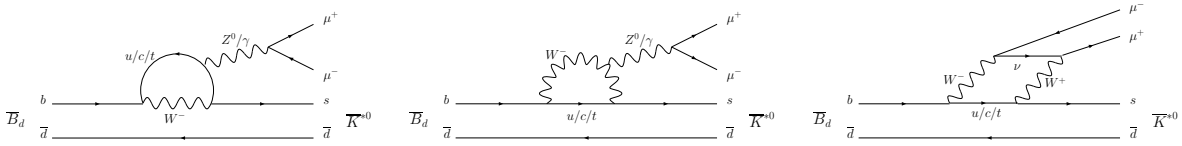

(a) Quark Penguin (b) W Penguin (c) W Box

Figure 1. SM Feynman diagrams for the $\overline{B}_d \to \overline{K}^{*0}\mu^+\mu^-$ decay.

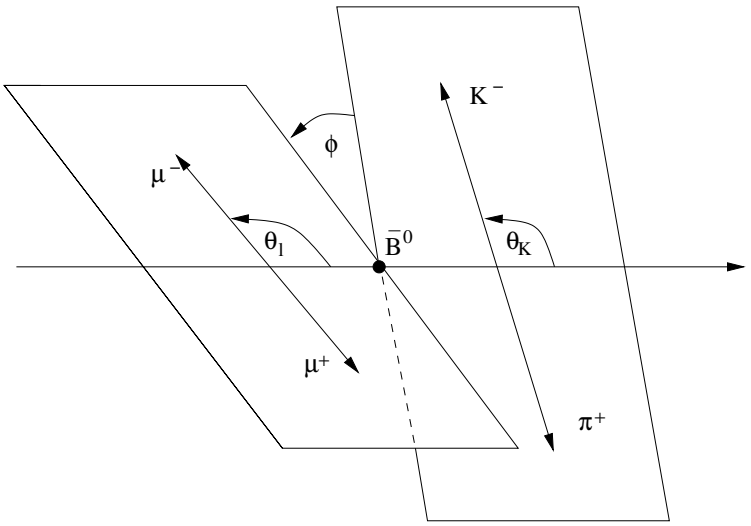

Figure 2. The angles used to describe the decay $\overline{B}_d \to \overline{K}^{*0}\mu^+\mu^-$. The z-axis is the direction in which the B meson flies in the rest frame of the $\mu^+\mu^-$. θ_l is the angle between the μ^- and the z-axis in the $\mu^+\mu^-$ rest frame, θ_K is the angle between the K^- and the z-axis in the $\overline{K}^*$ rest frame, and ϕ is the angle between the normals to the $\mu^+\mu^-$ and $K\pi$ decay planes in the B rest frame. For the B_d the angles are measured relative to the μ^+ and K^+.

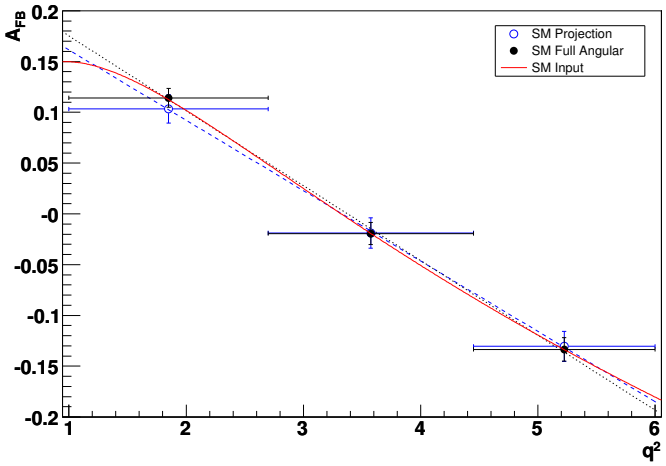

(a) A_{FB} Distribution

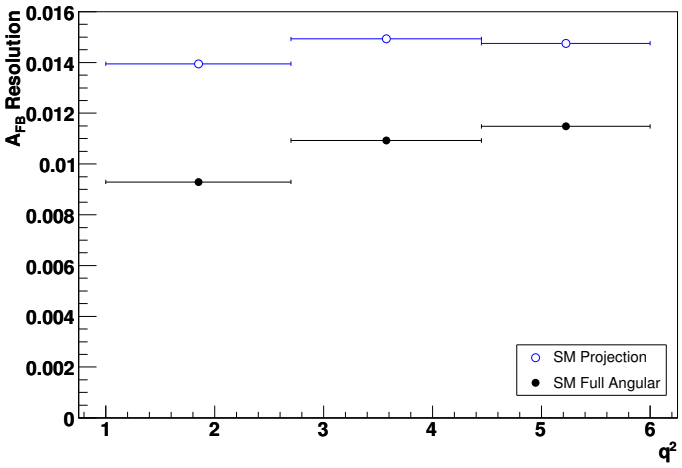

(b) A_{FB} Resolutions

Figure 3. Comparison between the full angular and projection fits for $10\,\mathrm{fb}^{-1}$ of SM data over three q^2 bins, 1.0–2.7 GeV^2/c^4, 2.7–4.45 GeV^2/c^4, and 4.45–6.0 GeV^2/c^4, chosen to give approximately equal numbers of signal events in each bin. (a) shows the A_{FB} distribution extracted from the full angular (closed points) and projection fits (open points). The x-values and their errors show the central value of the q^2 bin and its width, while the y-values and their errors show the mean value of A_{FB} over 1000 toy fits and the projected experimental resolution on the point. The solid line shows the SM input calculation and the dotted (dashed) line is a straight line fit to the full angular (projection) points. (b) shows explicitly the A_{FB} resolutions for comparison where the marker convention is the same as in (a).

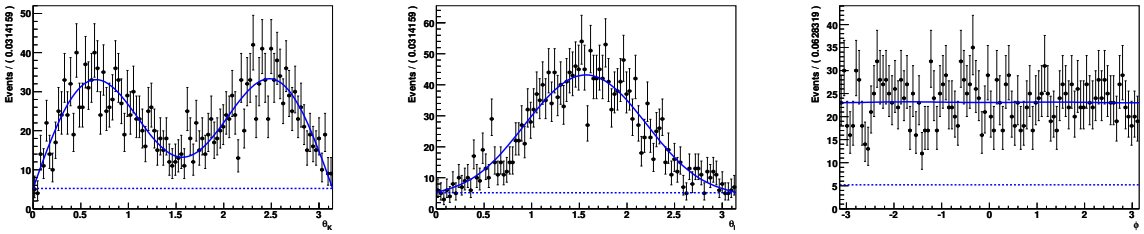

(a) θ_K (b)θ_l (c) ϕ

Figure 4. Numerical projections over the full angular decay distribution for the q^2 bin from 1–6 GeV^2/c^4 using SM NLO input values. The solid line shows the input model which includes both signal and background contributions while the dashed line shows only the background contribution. The points are an example 2 fb^{-1} toy data set generated from the model using an accept–reject algorithm.